Fetters, L. J., unpublished results). Thus, the parameter $\langle R^2\rangle/M$ was corrected to 75 °C and $T_g$ + 100 °C. A similar change in $\langle R^2\rangle/M$ for the two above temperatures was not done for PDMB since both theory and experiment indicate that d ln $\langle R^2\rangle/dT$ for sterreoirregular polydienes is ca. 0, e.g., see: Mays, J. W.; Hadjichristidis, N.; Graessley, W. W.; Fetters, L. J. *J. Polym. Sci., Polym. Phys. Ed.* **1986**, *24*, 2553 and references contained therein.
(34) Raju, V. R.; Rachapudy, H.; Graessley, W. W. *J. Polym. Sci., Polym. Phys. Ed.* **1979**, *17*, 1223.
(35) Doi, M. *J. Polym. Sci., Polym. Phys. Ed.* **1980**, *18*, 1005.
(36) The length $b$ can be estimated from $b^2 = \langle R^2\rangle/N$ where $N$ is the number of repeat units per chain.
(37) Reference 18, Appendix E, Section 6.

# On the Electrostatic Contribution to the Persistence Length of Flexible Polyelectrolytes

**Kenneth S. Schmitz* and Jae-Woong Yu**

*Department of Chemistry, University of Missouri—Kansas City, Kansas City, Missouri 64110.* *Received April 15, 1987; Revised Manuscript Received July 13, 1987*

ABSTRACT: Quasi-elastic light scattering methods were used to study the dynamics of dilute solutions of high molecular weight ($M_p = 10^7$ daltons) poly(acrylate) for $[KCl]_{added}$ = 0.00, 0.05, and 0.10 M. The correlation functions were analyzed by a third-order cumulant and an overlay histogram with exponential sampling methods of analysis. The histograms exhibited a bimodal distribution. It is argued that the fast mode evident in the histograms is associated with the pure translational diffusion process for PAA-K and that the slow mode may be associated with hindered diffusion through cages formed by neighboring polyions. The ionic strength dependence of the translational diffusion coefficient is interpreted in terms of a *minor increase* in both the excluded-volume parameter and the persistence length, where these parameters eventually reach a limiting value as the ionic strength is lowered. The failure of the current theoretical models of the electrostatic component to adequately describe this ionic strength dependence of the persistence length is discussed in detail.

## Introduction

The physical characteristics of polymer solutions are intimately associated with the flexibility of the polymer. The shear rate dependence of the viscosity, for example, is strongly affected by the flexibility characteristics of the polymer, where the more rigid and elongated polymers have the greater tendency to align with the hydrodynamic flow field. Variation of the solvent character greatly alters the statistical characteristics of the polymer. The effect of the solvent character is quantitatively defined, for example, by the scaling law parameter $\nu$, viz., $R_G \propto M_p^{\nu}$. A polymer in a good solvent is highly extended because of pairwise intrasegmental repulsion which leads to the Flory limit $\nu = 0.60$. A similar situation occurs in aqueous polyelectrolyte solution where the ionic strength is varied. Intuitively one would expect the polyelectrolyte to be highly extended in the limit of zero added salt due to the repulsion between the neighboring charged groups.

Interest in the persistence length of polyelectrolytes was stimulated by the studies of Manning counterion condensation onto the surface of rodlike polyions.[1-5] The interaction potential between the $i$th and $j$th groups on the same chain was assumed to be a screened Coulomb pairwise interaction, viz.,

$$V_{i,j} = (q_{net}/\epsilon)(|i-j|b)^{-1} \exp(-|i-j|b/\lambda_{DH}) \quad (1)$$

where $q_{net}$ is the net charge on the group, $\epsilon$ is the bulk dielectric constant, $b$ is the average spacing between neighboring charges, and $\lambda_{DH}$ is the Debye–Hückel screening length,

$$\lambda_{DH} = (1000/8\pi N_A \lambda_B I)^{1/2} \quad (2)$$

where $\lambda_B$ is the Bjerrum length,

$$\lambda_B = e^2/\epsilon kT \quad (3)$$

* To whom correspondence should be addressed.

$kT$ is the thermal energy, $N_A$ is Avogadro's number, $e$ is the magnitude of the elecron charge, $\epsilon$ is the bulk dielectric constant, and $I$ is the ionic strength of the solution,

$$I = (1/2)\sum_j Z_j^2 C_j \quad (4)$$

where $Z_j$ is the magnitude of the charge of the $j$th species of concentration $C_j$. A major conclusion drawn from the Manning theory in the linearized Poisson–Boltzmann limit is that counterions will condense onto the linear structure if $b < \lambda_B$; i.e., the maximum linear charge density that can be supported by the solvent is given by the Bjerrum length. The "transition" at which counterion condensation will occur is when the Manning parameter $\xi_M = \lambda_B/b$ becomes unity. A similar conclusion was made by Russel[6] for the nonlinearized Poisson–Boltzmann expression.

Skolnick and Fixman[7] and Odijk[8] independently examined the electrostatic component to the persistence length by using a mean-field approximation in the limit of the rigid-rod configuration. The major assumption in these models was that the polyelectrolyte undergoes minor deviations from the rodlike configuration such that one can express the elastic constant for bending, $\gamma$, as the sum of two terms, an intrinsic part $\gamma_0$ and an electrostatic part $\gamma_{el}$, as given by Yamakawa,[9] viz.,

$$\gamma = \gamma_0 + \gamma_{el} \quad (5)$$

It is further assumed that $\gamma_{el}$ is independent of the radius of curvature. Hence the potential of energy of bending is given by

$$\langle V\rangle = \left\langle (1/2)\gamma_0 \int_0^L (\partial^2 r/\partial s^2)^2 \, ds \right\rangle + \left\langle (1/2)\gamma_{el} \int_0^L (\partial^2 r/\partial s^2)^2 \, ds \right\rangle \quad (6)$$

Upon defining the persistence length by the wormlike coil model as $L_p = \gamma kT$, it follows from eq 5 that

$$L_p = L_0 + L_{el} \quad (7)$$

0024-9297/88/2221-0484$01.50/0 

and from eq 6 that

$$\langle V\rangle_{el} \propto L_{el} \tag{8}$$

Skolnick and Fixman[7] and Odijk[8] assumed only *small deviations* from the rodlike configuration and expanded the intersegment distance $|i - j|b$ in a Taylor series expansion about the rodlike parameters,

$$b_{ij} \sim |i - j|b[1 - [(|i - j|b)^2/12R_c^2]]^{1/2} \tag{9}$$

where $R_c$ is the curvature of the rod. The Skolnick–Fixman/Odijk (SF/O) form for $L_{el}$ in the *infinite chain length limit* $L/\lambda_{DH} \gg 1$ is

$$L_{el} = \lambda_B\lambda_{DH}^2/4b^2 = \xi_M^2\lambda_{DH}^2/4\lambda_B \qquad (\xi_M < 1) \tag{10}$$

Odijk and Houwaart[10] later suggested in an ad hoc manner that for $\xi_M > 1$, one should substitute $\lambda_B$ for $b$, with the result

$$L_{el} = \lambda_{DH}^2/4\lambda_B \qquad (\xi_M > 1) \tag{11}$$

Odijk[11] extended some of the above ideas to the solution properties of flexible polyelectrolytes in the limit of zero added salt. Under these conditions it is only the dissociated counterions that contribute to the screening length $\lambda_{DH}$, thus

$$C_c = |Z_p|C_p \tag{12}$$

where $C_c$ is the molar concentration of counterions, $C_p$ is the molar concentration of polyions, and $|Z_p|$ is the magnitude of the polyion charge. For dilute solutions in which $\lambda_{DH} \gg L$, the polyion may be assumed to be in a highly extended form since $L_{el} \gg L$ in accordance with eq 10 and 11. As the polyion concentration is increased, $C_c$ is likewise increased in accordance with eq 12 and $\lambda_{DH}$ is correspondingly decreased. Odijk argued that a transition from a rodlike to a coillike conformation of the flexible polyion occurs when $L_{el} = L$, since a further increase in $C_p$ would result in the inequality $L_p = L_{el} < L$ and a decrease in intrasegment repulsion due to an increase in the screening efficiency. The molar polyion concentration at which $L_{el} = L$ is obtained from eq 2, 10, and 12,

$$C^*_p = 1000/(16\pi N_A L^2\langle b\rangle) \tag{13}$$

where $\langle b\rangle$ is the average spacing between charges ($\langle b\rangle = b$ if $\xi_M > 1$ and $\langle b\rangle = \lambda_B$ if $\xi_M < 1$), $|Z_c| = 1$, and $|Z_p| = L/\langle b\rangle$.

The Manning condensation model has been tested by Zimm and Le Bret[12,13] in their computer-generated solutions to the complete Poisson–Boltzmann equation, where they examined the effect of geometry on the counterion condensation phenomenon. Their results indicated that there is a finite number of counterions that cannot be "diluted away" from the rod geometry, regardless of the volume of the solution. This fraction of residual counterions is the same as predicted by the Manning model, hence they are said to be condensed. Using the criterion that "undilutable" counterions are condensed, Zimm and Le Bret concluded that *all* of the counterions are condensed *for the plane geometry* and that *none* of the counterions are condensed *for the spherical geometry*.

The transition criterion ($\xi_M = 1$) was experimentally verified by the electrophoretic light scattering studies of Klein and Ware[14] on poly[(dimethylamino)hexylene bromide] in aqueous solution with methanol addition such that $0.82 < \xi_M < 1.85$.

Le Bret[15] and Fixman[16] examined the effect of a finite cylinder radius on ionic strength dependence of the persistence length. Le Bret[15] used a toroid model in the limit of large curvature for cylinders with a conducting surface and a nonconducting surface. The appropriate Poisson–Boltzmann equation was solved numerically by a multipole expansion for small surface charges and a two-dimensional grid for the higher charged surfaces. These calculations were performed as a function of $\xi_M$ and $a/\lambda_{DH}$ for nonconducting and conducting surfaces. In the case tailored for DNA ($\xi_M = 4.2$ and $a = 10$ Å), the electrostatic component of the persistence length for $a/\lambda_{DH} = 0.01$ was reported to be 24.124 and 23.943 Å respectively for the nonconducting and conducting surface limits. By comparison, eq 10 and 11 yield the values 618.080 and 35.038 Å, respectively, for $\lambda_B = 7.135$ Å (25 °C). Fixman[16] used analytical expressions in a power series in $\lambda_{DH}/R$ and cos ($\theta$) for deviations from a rodlike structure, where $R$ is the curvature and $\theta$ is the bending angle. Calculations were performed for the dielectric constant ratios $\epsilon_I/\epsilon_O = 0$ and 1, where the subscripts I and O denote the inside and outside cylindrical regions. The results were presented in terms of the ratio $L_p/L_p(\text{cond})$ as a function of $a/\lambda_{DH}$, where $L_p(\text{cond}) = \lambda_{DH}^2/4\lambda_B$ is the Debye–Hückel limit with counterion condensation (cf. eq 11). For $a = 10$ Å and $\epsilon_I/\epsilon_O = 0$, Fixman calculated for the 1:1 salt the values $L_p/L_p(\text{cond}) = 0.6878$ and 1.482 respectively for $\lambda_{DH} = 1000$ and 100 Å. As pointed out by Fixman, the results of Le Bret were in good agreement except for the extremely low ionic strength conditions. A major finding of both studies is that the ionic strength dependence of $L_{el}$ is stronger than indicated by the Debye–Hückel limiting expression with counterion condensation (cf. eq 11).

All of the above theoretical studies have focused exclusively on the ionic strength dependence of the persistence length for linear and cylindrical configurations that exercise small deviations from the rodlike limit. These theories have been successfully applied, to a greater or lesser extent, to the description of the ionic strength dependence of $L_{el}$ for DNA. Since the intrinsic persistence length of DNA is on the order $L_0 \sim 500$ Å, the inequality $L_{el} < L_0$ holds for most experimental conditions in the literature since the ionic strength is generally greater than $10^{-3}$ M.

The subject of the present study is on the ionic strength dependence of $L_{el}$ for very flexible polyions, where $L_0 \leq L_{el}$. The model system chosen for this initial investigation is poly(potassium acrylate) (PAA-K), where it was reported[17] that 10 Å $< L_0 <$ 13 Å and 1 Å $< a <$ 2.5 Å.

## Methods

**Materials.** Poly(acrylic acid) (PAA) was synthesized in the laboratory of Dr. Oh-Kil Kim of the Naval Research Laboratory, where the synthesis procedure was previously described.[18] The average molecular weight of the preparation used in these studies was given as $M_p = 10^7$ daltons. The stock solution was in deionized water at a concentration of 0.024 g/L (24 ppm) at pH 8.0.

The ionic strength of the solutions was adjusted by addition of one part of the appropriate stock KCl solution, made up in deionized water, to nine parts of the stock solution of PAA.

**Quasi-Elastic Light Scattering.** The cylindrical light scattering cells were cleaned in dilute solutions of hot nitric acid prior to their use in the experiment. Since the PAA-K solutions were very dilute, contamination by dust was minimized by using a specially designed box which was closed to the outside during the filtration procedure. The system was flushed with several cell volumes of double-distilled water by using a gravity flow filtration system. This was followed by a rinse of two cell volumes with the appropriate solvent, and then a portion of the PAA-K solution was gravity flow filtered to rinse the cell to min-

imize additional dilution that might result from residual solvent. The final concentration of PAA-K for all of the solutions was 20–22 ppm.

The quasi-elastic light scattering apparatus was vibration isolated by means of a pnuematic optical table. The incident light source was the 488-nm line of a Spectra Physics Model 2025-03 argon ion laser operating at a power of ~100 mW. The scattered light was detected by an RCA 7265 PMT, and the resulting phototube signal was relayed to a Langley-Ford 1096 autocorrelator. The correlation function was then sent to a Hewlett-Packard 86A microprocessor and stored on floppy disks for future analysis.

**Data Analysis.** The correlation functions were analyzed by the method of cumulants[19] and the Fletcher–Ramsay[20] method of overlay histograms with exponential sampling.

The cumulant analysis was carried out to the third order by using the mathematical form

$$C(t) = A \exp[-K_1 t + (K_2/2)t^2 - (K_3/6)t^3] + B \quad (14)$$

where $A$, $B$, and the $K_i$ are adjustable parameters determined by an iterative nonlinear least-squares program developed in our laboratory, using the criteria that changes in all five of the adjustable parameters must be less than 0.5% before the values be deemed acceptable. The first cumulant, $K_1$, for the homodyne correlation function is related to the apparent diffusion coefficient $D_{app}$ by

$$D_{app} = K_1/2K^2 \quad (15)$$

where $K$ is the scattering vector for the scattering angle $\theta$,

$$K = (4\pi n/\lambda_0) \sin(\theta/2) \quad (16)$$

$n$ is the index of refraction, and $\lambda_0$ is the wavelength of incident light in a vacuum.

The Fletcher–Ramsay overlay histogram method assumes that the correlation function is of the form

$$C(t) = \left[\int_0^\infty G(\gamma_i) \exp(-\gamma_i t)\, d\gamma_i\right]^2 + 1 + \epsilon(t) \quad (17)$$

where $G(\gamma_i)$ is the relative amplitude of the $i$th mode having the decay rate $\gamma_i$ and $\epsilon(t)$ represents random fluctuating noise. This is an operator-interactive method in which the central value of $\gamma$, the multiplier $M$ in the exponential sampling procedure, and the number of steps are the input parameters. The values of $\gamma_i$ are then generated by

$$\gamma_n = M\gamma_{n-1} \quad (18)$$

A number of generated histograms that differ only in the central value of $\gamma$ are then normalized and superimposed to provide the final histogram for further analysis.

## Results

**Cumulant Analysis.** The first cumulant for aqueous solutions of PAA-K for added salt concentrations of [KCl] = 0.00, 0.05, and 0.10 M was determined from the third-order cumulant analysis expression given by eq 14. Data were collected at several delay intervals $\Delta t$ over the range 100 $\mu$s < $\Delta t$ < 1000 $\mu$s. The average value and the standard deviation for all data taken at selected angles are summarized in Table I. The relatively large standard deviations are a direct result of averaging over all of the delay intervals and do not reflect the precision obtained for data at any one delay interval. The angle dependence for each of these solutions is characteristic of internal modes and/or size polydispersity, where the weight-average amplitudes favor the smaller species at the higher scattering angles.

**Table I**
**First Cumulant[a] for PAA-K Solutions at 25 °C**

| | $K_1 \pm \sigma_{sd}$, 1/s [$D_{app} \times 10^9$, cm$^2$/s] with [KCl]$_{added}$ | | |
|---|---|---|---|
| $\theta$ | 0.00 | 0.05 | 0.10 |
| 40° | 107 ± 11 [3.88] | 145 ± 18 [5.26] | 205 ± 36 [7.44] |
| 50° | | 219 ± 43 [5.20] | |
| 60° | 242 ± 21 [4.12] | 285 ± 49 [4.84] | 325[b] [5.52] |
| 70° | | 395 ± 86 [5.10] | |
| 90° | 329 ± 35 [2.79] | | |

[a] These values represent average values of several data collection intervals in which the correlation function was analyzed by a third-order cumulant analysis routine with a floating base line. The apparent diffusion coefficient is $D_{app} = K_1/2K^2$. [b] Only one measurement.

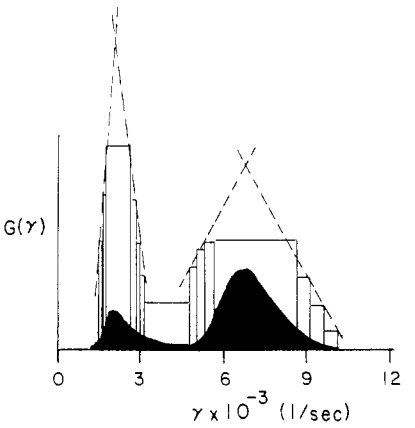


**Figure 1.** Overlay histogram/exponential sampling analysis of simulated bimodal correlation function without added noise. The solid area is the input distribution of the amplitudes for the simulated correlation function. The method for generating the simulated function is described in the text. The dashed lines illustrate the extrapolation method for obtaining the average decay rate for each mode.

These data also indicate a possible ionic strength expansion of the polyion dimensions as the ionic strength is lowered.

**Overlay Histogram Analysis.** In order to assess the validity of the overlay histogram method of analysis, we generated correlation functions composed of 70 exponential functions with a known distribution of amplitudes and decay rates. The amplitudes $a_i$ were generated by the function

$$a_i = A \exp[-B[(y - \langle y\rangle)/\langle y\rangle]^2] \quad (19)$$

where $A$ is an arbitrary constant that denotes the relative contribution of the family of functions associated with a particular mode, $B$ is an adjustable parameter that determines the width of the distribution about the average value $\langle y\rangle$, and $y$ represents either the decay rate or relaxation time. Functions were generated both without and with added random noise, viz., $\epsilon(t)$ in eq 17. In the present simulation, the correlation functions were bimodal and the relaxation times ($y$) were linearly spaced. Each mode was composed of 35 exponential functions, with the following parameters: $A_f = 0.67$, 100 $\mu$s < $y_f$ < 200 $\mu$s, $\langle y\rangle$ = 150 $\mu$s, $B_f = 26.96$; $A_s = 0.33$, 200 $\mu$s < $y_s$ < 800 $\mu$s, $\langle y\rangle$ = 500 $\mu$s, $B_s = 8.32$. The random noise $\epsilon(t)$ was generated by a random number generator and then adjusted so that $\langle\epsilon(t)\rangle = 0$ for the function under consideration.

The Fletcher–Ramsay overlay histogram analysis result for a representative simulated correlation function without added noise is shown in Figure 1, where $G(\gamma)$ is plotted as a function of $\gamma$. The shaded area represents the input amplitude distribution, which appears to be faithfully reproduced by the overlay histogram method. In order to estimate the *average* decay rate for each mode, $\gamma_{av}$, we have

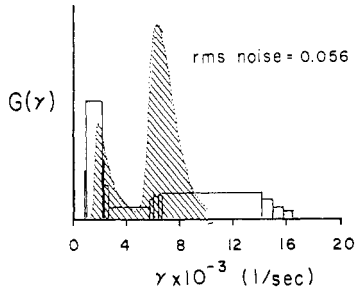


**Figure 2.** Overlay histogram/exponential sampling analysis of simulated bimodal correlation function without added noise. Random noise with a root-mean-square amplitude of 0.056 was added to the correlation function analyzed in Figure 1. The effect of the added noise is to introduce a "repulsive interaction energy" between the two modes.

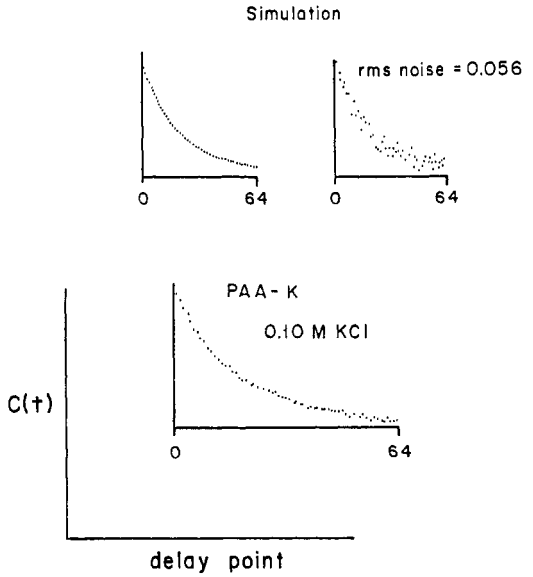


**Figure 3.** Comparison of the quality of correlation functions. A typical correlation function for the PAA-K system is compared with the simulated correlation functions. As indicated above, the experimental correlation functions are better represented by the simulated correlation function without noise.

used the intersection point of the extrapolated tangents to the step edges on both sides of the distribution as shown in this illustration. The overlay histogram analysis of the correlation function with added noise with a root-mean-square deviation of 0.056 is shown in Figure 2. These results indicate that the effect of noise is to "split" the resulting bimodal distribution, where the maximum in the distributions for the fast and slow decay modes are shifted to higher and lower values, respectively. That is, noise seems to introduce a "repulsive" interactions between the modes of a bimodal distribution.

The above results clearly indicate that the quality of the correlation function greatly affects the interpretation of the histogram analysis results. Shown in Figure 3 are two simulated correlation functions, with and without added noise, along with a representative correlation function for PAA-K. Since the PAA-K correlation function is better represented by the simulated correlation function without noise, or rather does not exhibit nearly the noise level of the simulated correlation function with added noise, it is suggested that the overlay histogram analysis of the PAA-K correlation functions provides a realistic representation of the amplitude distribution for these functions.

Overlay histograms for PAA-K at the two ionic strength extremes, $[KCl]_{added}$ = 0.00 and 0.10 M, are illustrated in Figure 4. All of the correlation functions analyzed by this

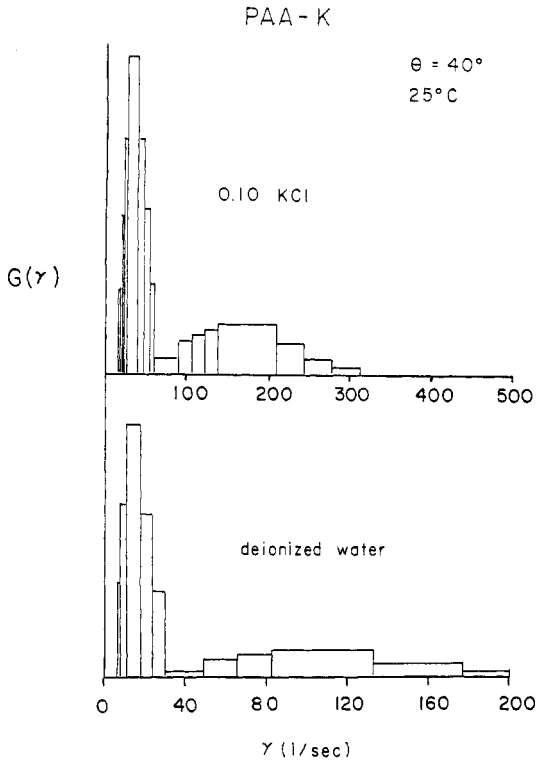


**Figure 4.** Overlay histogram/exponential sampling results for PAA-K at the two added salt extremes.

**Table II**
**$D_{app}{}^a \times 10^9$ for PAA-K Solutions at 25 °C**

| | $[KCl]_{added}$ | | | | | |
|---|---|---|---|---|---|---|
| θ | 0.00 | 0.05 | 0.10 | 0.00 | 0.05 | 0.10 |
| 40° | 8.05 | 9.36 | 12.6 | 1.28 | 1.65 | 2.42 |
| 50° | | 10.9 | | | 1.1 | |
| 60° | 7.67 | 9.23 | 11.5 | 1.32 | 1.28 | 1.57 |
| 70° | | 8.95 | | | | |
| $\langle D_{app}\rangle^b \times 10^9$ | 7.86 | 9.61 | 12.1 | 1.30 | 1.34 | 2.00 |
| $R_H$, Å$^c$ | 3120 | 2550 | 2030 | 18900 | 18300 | 12300 |

$^a D_{app} = \langle \gamma_{av}\rangle/K^2$ (cm²/s), where $\gamma_{av}$ was determined by the tangent extrapolation method and $\langle\ \rangle$ denotes the average of data at the specific angle θ. $^b \langle D_{app}\rangle$ is the average of all data at all scattering angles. $^c R_H = (kT/6\pi\eta D_{app}) \times 10^8$.

method exhibited a bimodal distribution. The apparent diffusion coefficient for each mode is defined as

$$D_{app} = \gamma_{av}/K^2 \tag{20}$$

Values for $D_{app}$ at a few scattering angles are summarized in Table II, along with the overall average $\langle D_{app}\rangle$ and effective hydrodynamic radius $R_H$,

$$R_H = kT/6\pi\eta\langle D_{app}\rangle \tag{21}$$

## Discussion

**Interpretation of the Bimodal Distribution.** In view of the high molecular weight of the PAA-K used in these studies, it may be that the observed bimodal distribution is due to the "pure" translational relaxation mode and a "mixed" translational–internal relaxation mode. In the case of neutral macroparticles, the relationship between these two decay rates is

$$\gamma_{fast} = \gamma_{slow} + \Delta \tag{22}$$

where the slow decay rate is related to the translational diffusion coefficient $D_0$ by

$$\gamma_{slow} = D_0K^2 \tag{23}$$

and $\Delta$ represents an internal decay rate. Since caution should be exercised in the interpretation of polyelectrolyte data, we first compare the experimental values of $\gamma_{fast}$ and $\gamma_{slow}$ for the 0.10 M KCl sample (to minimize electrostatic effects since $\lambda_{DH}$ = 9.7 Å) with those expected for the rigid cylinder and the wormlike coil under $\Theta$ conditions. In making this comparison it is assumed that any differences between the theoretical and experimental results are small (within a factor of 4) and can be attributed to the polyelectrolyte nature of PAA. The appropriate molecular parameters are estimated from the values of Kitano et al.[17] for the mass/length ratio of 40 g/Å and the *upper limit* diameter value $d$ = 5 Å for PAA under $\Theta$ conditions (neutralized preparation in 1.5 M NaBr). The contour length for $M_p = 10^7$ is therefore $L = 2.5 \times 10^5$ Å. In view of the fact that $L/d = 5 \times 10^4 \gg 1$, end effects are neglected in the following development.

In the case of the rigid cylinder, $\Delta$ is identified with the decay rate for orientational relaxation of the $j$ = 2 harmonic mode about the small axis,[21]

$$\Delta = 6D_\theta \tag{24}$$

where one has for the rotational diffusion coefficient[22]

$$D_\theta = 3kT \ln (L/d)/\pi\eta L^3 \tag{25}$$

The translational diffusion coefficient for a rigid cylinder is given by[22]

$$D_0 = kT \ln (L/d)/3\pi\eta L \tag{26}$$

Using eq 24–26, one can write $\Delta$ in terms of $D_0$ for the rigid cylinder

$$\Delta = 54D_0/L^2 \tag{27}$$

In the case of the wormlike coil model, the mean-square end-to-end displacement $\langle r^2 \rangle$ is

$$\langle r^2 \rangle = (2LL_p)[1 - [1 - \exp(L/L_p)](L_p/L)] \tag{28}$$

where the persistence length is assumed to have an intrinsic part and an electrostatic part as given by eq 7. Kitano et al.[17] reported the value $L_0 \sim 10$ Å, which gives for this preparation the ratio $L/L_p = 2.5 \times 10^4$ in the 0.1 M KCl solution. One may therefore use the flexible coil value of $\langle r^2 \rangle = 2LL_p$ and the relationships

$$\langle R_G^2 \rangle = \langle r^2 \rangle/6 = LL_p/3 \tag{29}$$

and, for the conversion to the hydrodynamic radius,[23]

$$\langle R_G^2 \rangle^{1/2} = 1.5R_H \tag{30}$$

The internal relaxation times $\tau_n$ for the flexible coil can be expressed in terms of $D_0$[24]

$$\tau_n = \langle r^2 \rangle/3\pi^2 n^2 D_0 \tag{31}$$

Combining eq 29–31 and assuming $\Delta$ is to be associated only with the slowest relaxation time, viz., $\Delta = 2/\tau_1$,[24] one has for the flexible coil model

$$\Delta = (16D_0^3\pi^4)/(kT/\eta)^2 \tag{32}$$

The experimental value for $D_0$ is given by eq 23 for the 0.1 M KCl solution. The theoretical value for $D_0$ is obtained by combining eq 21, 29, and 3.0; viz.,

$$D_0 = (kT/4\pi\eta)(3/LL_p)^{1/2} \tag{33}$$

The results of the calculations are summarized in Table III and are to be compared with the experimental values given in Table II.

The theoretical value for the translational diffusion coefficient for the rigid cylinder is virtually identical with the experimental value of $2 \times 10^{-9}$ cm²/s for the slow mode in the 0.1 M KCl solvent. While this agreement is quite good for the slow mode, the *theoretical* value for $\Delta$ is 4 orders of magnitude *smaller* than the experimental value. If the fast mode is to be associated with the rigid cylinder translation–rotation coupled mode, then one would have to postulate a mechanism which greatly enhances the rotational motion of the cylinder while leaving the pure translational mode unaffected. Furthermore, if the PAA-K is fully extended in the 0.1 M KCl solvent, what might account for the *decrease* in $D_0$ upon lowering the ionic strength? One possible interpretation of this observation is that the "effective" diameter of the cylinder increases as the ionic strength is lowered due to an extension of the Debye–Huckle cloud. This possibility is ruled out, however, when one considers the required magnitude of the effective diameter in relationship to the ion cloud thickness. In order to account for the change in $D_0$ in going from 0.10 M KCl to 0.05 M KCl, the effective diameter must go from a value of 5 to 269 Å. In view of the fact that the Debye–Hückel screening length is on the order of 14 Å, this value for the effective diameter is clearly unphysical. One likewise cannot interpret the decrease in $D_0$ as being due to interparticle interactions since a decrease in the ionic strength should increase the mutual diffusion coefficient of particles with like charge.[25] It is concluded, therefore, that the bimodal distribution does not reflect the dynamics of a rigid cylindrical particle.

**Table III**
**Analysis of the Bimodal Distribution of PAA-K in 0.1 M KCl at 25 °C**

| experimental | $\theta$ = 40° | 50° | 60° |
|---|---|---|---|
| $\gamma_{fast}$, 1/s | 174 | 229 | 340 |
| $\gamma_{slow}$, 1/s | 33 | 20 | 46 |
| $\Delta_{exp}$,[a] 1/s | 141 | 209 | 294 |
| $(\Delta_{exp}/K^2) \times 10^8$, cm²/s | 1.02 | 1.00 | 1.00 |

| theoretical[g] | $D_0 \times 10^9$, cm²/s | $D_\theta \times 10^3$, 1/s | $\Delta$, 1/s |
|---|---|---|---|
| cylinder | 2.12[b] | 3.05[c] | 0.018[d] |
| coil | 40.3[e] | | 4778[f] |

[a] $\Delta_{exp} = \gamma_{fast} - \gamma_{slow}$. [b] Computed from eq 26. [c] Computed from eq 25. [d] Computed from eq 27. [e] Computed from eq 33. [f] Computed from eq 32 and 33. [g] Computed with the values $L = 2.5 \times 10^5$ Å, $L_0 = L_p = 10$ Å, and $d = 5$ Å.

In the case of the flexible coil, the apparent hydrodynamic radius calculated from eq 29 and 30 is $R_H = (LL_p/3)^{1/2}/1.5 \sim 609$ Å, which gives a value of $D_0$(25 °C) $\sim 40.3 \times 10^{-9}$ cm²/s. It is highly unlikely that a reduction of this value by a factor of ~20 as required to obtain $\langle D_{app} \rangle_{slow}$ can be accounted for under these solvent conditions where $\lambda_{DH} \sim 10$ Å. On the other hand, the ratio $\langle D_{app} \rangle_{fast}/(D_0)_{coil} \sim 0.3$ might be accounted for by polyelectrolyte effects on the persistence length and/or excluded volume associated with the polyion dimensions. If the *fast mode* is to be associated with the *pure translational motion*, then there is at this time no theoretical expression relating $\gamma_{fast}$ and $\gamma_{slow}$. The observation that $\Delta_{exp}/K^2$ is independent of the scattering angle, at least over the range $40 < \theta < 60$, indicates that $\gamma_{slow}$ is to be associated with a translational motion (cf. Table III).

If both decay modes are related to translational motions, then in principle one might expect to also observe internal relaxation processes in the overlay histograms as well. It is not possible to distinguish internal processes if they do exist for the slow relaxation mode *in the presence of the fast mode* since a resolution on the order of a few hertz is required. In regard to the fast mode the pure translation and coupled translation–internal modes might be sufficiently separated to be observed as indicated by the the-

oretical values for $D_0$ and $\Delta$ given in Table III. One must consider both the *amplitude* and the *decay rate* of the coupled mode process at the angles employed in this study. Assuming that eq 30 is valid, the largest value of the product $\langle R_G^2\rangle^{1/2}K$ in these studies is for zero added salt at the scattering angle of 60°, giving the value $\langle R_G^2\rangle^{1/2}K = (1.5)(3120 \times 10^{-8})(1.7 \times 10^5) \sim 8.0$. According to the calculations of Pecora,[24] the amplitude of the coupled mode is sufficiently large to be observed. The internal relaxation rate $\Delta$ is estimated from eq 32 by using the experimental value of $\gamma_{fast}$, assumed to be the pure translational process, and eq 20. The estimated value for $\Delta$ is therefore $\sim 33\ s^{-1}$. Unlike smaller molecules whose lower order internal motions decay at a rate comparable to or faster than their translational motions, the *lower order* internal modes of very large particles are somewhat sluggish and their resolution on the basis of exponential sampling procedures for inverse Laplace transformation methods is therefore virtually impossible to achieve. Their presence may partially account for the "high-frequency tail" observed in the overlay histograms for both modes, where the other contributing features are size polydispersity and the fact that exponential sampling methods result in steps that favor the high-frequency region. The presence of an internal mode should not drastically affect the values of $\langle\gamma\rangle_{av}$ obtained by the extrapolation method employed when one takes into consideration the relative magnitudes of the amplitudes associated with the various internal modes.

It is the thesis of the analysis that follows that the fast relaxation mode is associated with the "single-particle" diffusion process and that the slow mode is a manifestation of "hindered" collective motions of particles as might result from the formation of solute "cages".

**The Fast Relaxation Mode.** In order to interpret the fast mode, we use the expression for the radius of gyration derived by Sharp and Bloomfield[26] in which the persistence length and excluded-volume parameters are explicitly stated. Converting their notation to the present notation [$\sigma = L$; $1/2\lambda = L_p$; and $\epsilon = 2\nu - 1$ (excluded-volume parameter)], the square root of their eq 16 becomes

$$\langle R_G^2\rangle^{1/2} = [(1/2L_p)^{(\nu-1)}L^\nu/[(2\nu+1)(2\nu+2)]^{1/2}] \times [1 - (\nu+1)/(\nu L/L_p)]^{1/2} \sim [(1/2L_p)^{(\nu-1)}L^\nu]/[(2\nu+1)(2\nu+2)]^{1/2} \quad (34)$$

where the inequality $(\nu+1)/(\nu L/L_p) \ll 1$ was employed since $L/L_p \gg 1$ for the present system. In general both $L_p$ and $\nu$ may be sensitive to the ionic strength and charge density of the polyelectrolyte. In the analysis which follows the $\Theta$ state is used as the reference conformation. Under $\Theta$ conditions there are no exclude-volume effects, hence $\nu = 0.5$. Equation 34 reduces to

$$\langle R_G^2\rangle_0^{1/2} = (LL_p/3)^{1/2} \quad (35)$$

Using the value $L_p = 10$ Å,[17] one calculates from eq 35 the value $\langle R_G^2\rangle^{1/2} = 913$ Å, and from eq 30 $R_H = 609$ Å for the reference state of the present sample of PAA. The $\Theta$ condition obtains for the PAA system in 1.5 M added salt conditions as indicated by light scattering[27] and viscosity[28] measurements. The upper limit value of $\nu$ is not obvious in a polyelectrolyte system. The Flory limit of $\nu = 0.6$ obtains for a mean-field approach for pairwise interactions between internal segments. The Flory limit might be exceeded for polyelectrolytes with complex intrastrand interactions where the exponential law for the rodlike configuration would be considered the asymptotic upper limit.

The *upper bounds* for the parameters $\nu$ and $L_{el}$ are estimated from $R_H/(R_H)_0 = \langle R_G^2\rangle^{1/2}/\langle R_G^2\rangle_0^{1/2}$ for the present system by using $(R_H)_0 = 609$ Å and $L = 2.5 \times 10^{-5}$ Å in eq 34, giving

$$R_H/(R_H)_0 = [0.00328L_p(1.25 \times 10^5/L_p)^\nu]/[(2\nu+1)(2\nu+2)]^{1/2} \quad (36)$$

An upper limit for $L_p$ is obtained by setting as constant the value $\nu = 0.5$, with the resulting expression for eq 36

$$R_H/(R_H)_0 = 0.474(L_p)^{1/2} \quad (37)$$

An upper limit for $\nu$ is obtained by setting $L_p = 10$ Å as a constant value, in which case eq 36 becomes

$$R_H/(R_H)_0 = [0.0328(1.25 \times 10^4)^\nu]/[(2\nu+1)(2\nu+2)]^{1/2} \quad (38)$$

**Table IV**
**Comparison of Upper Bound Experimental and Theoretical Values of the Electrostatic Persistence Length at 25 °C**

| | $C_s$, M $[a/\lambda_{DH}]$ at length, Å | | |
|---|---|---|---|
| | $7 \times 10^{-5}$ [a] | 0.05 | 0.10 |
| $\lambda_{DH}$ | 367 | 13.7 | 9.7 |
| $L_{el}$ [b] | 250 | 166 | 101 |
| $L_{el}$ [c] | 146000 | 204 | 102 |
| $L_{el}$ [d] | 9635 | 13 | 7 |
| $L_{el}$ [e] | 4190 [0.019] | 209 [0.70] | 199 [1.00] |
| $L_{el}$ [e] | | 31.2 [0.17] | 25.3 [0.25] |
| $L_{el}$ [f] | 1460 [0.019] | 14 [0.70] | 6.1 [1.00] |
| $L_{el}$ [g] | 1495 [0.019] | 110 [0.70] | 97.6 [1.00] |

[a] Estimated from eq 12 with Manning condensation; $|Z_p| = L/b$ with $b = 7.1$ Å and $M_p = 1 \times 10^7$. [b] Estimated from eq 7, 29, and 30 with $L_0 = 10$ Å. [c] Calculated from eq 10 with $\xi_M = 4$. [d] Calculated from eq 11. [e] Calculated from Fixman's ratio $L_{el}/L_{cond}$, where $L_{cond}$ is identified with eq 11 of this text. [f] Estimated from Le Bret[15] for a conducting surface. [g] Estimated from Le Bret[15] for a nonconducting surface.

**Upper Bound for the Electrostatic Persistence Length.** Upper bound values of $L_{el}$ estimated from eq 7 and 37 are given in Table IV for the three ionic strengths used in this study. These values were compared with the values calculated from the SF/O expression (cf. eq 10) and the Odijk–Houwaart expression (cf. eq 11). The experimentally estimated values of $L_{el}$ were also compared with the numerical results of Le Bret[15] and Fixman.[16] Since these authors tailored their calculations for DNA by using a cylindrical radius of $a = 10$ Å presented in terms of the dimensionless parameter $a/\lambda_{DH}$, the comparison was made of interpolated values of $L_{el}$ obtained by a graphical presentation of the calculations for $a = 2.5$ Å with the listed values for $a = 10$ Å. As indicated in the paragraph below, this simple conversion between polyions of different diameters may be questioned for nonconducting cylindrical surfaces in the high ionic strength regime. Le Bret also tabulated the results for different values of the Manning parameter $\xi_M$ other than the DNA value of 4.2. Since the Manning parameter for PAA-K is sufficiently close to that for DNA, i.e., $\xi_M$(PAA-K) $= 7.135/1.8 \sim 4$, there was no adjustment of the Le Bret and Fixman results to take into consideration this slight difference in values of $\xi_M$. The results of these comparisons are summarized in Table IV.

In regard to the relative values of the numerical calculations of Le Bret and Fixman as compared with those of the SF/O mean-field theories, it is interesting to note that (1) the mean-field values for $L_{el}$ are considerably larger than those obtained by numerical analysis (2) and there exists a crossover region in which the mean-field theories yield smaller values of $L_{el}$ than the numerical models. This behavior appears to bring into question the simple conversion from one polyion diameter to another as inferred from the presentation of the data in the form of the di-

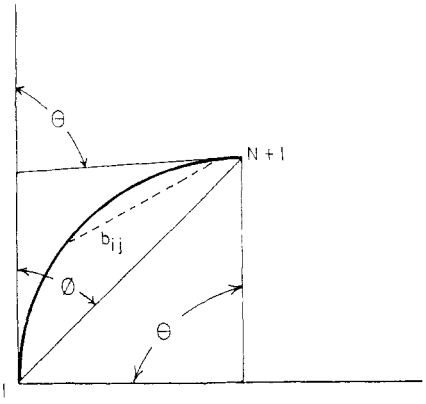


**Figure 5.** Schematic representation of the bent rod.

mensionless parameter $a/\lambda_{DH}$. Consider, for example, the paper of Le Bret[15] in which the following equations are given ($\kappa = 1/\lambda_{DH} \propto C_s^{1/2}$): $\kappa_2 a_2 = \kappa_1 a_1$ (eq 1.27); $L_{el}(\xi_M, \epsilon, \kappa_2, a_2) = (a_2/a_1)^2 L_{el}(\xi_M, \epsilon, \kappa_1, a_1)$ (eq 1.28). Clearly, these simultaneous expressions yield $L_{el}(\xi_M, \epsilon, \kappa_2, a_2) = (\kappa_1/\kappa_2)^2 L_{el}(\xi_M, \epsilon, \kappa_1, a_1)$ or $(L_{el})_2/(L_{el})_1 = (C_s)_2/(C_s)_1$, which is precisely the result of the SF/O mean-field models.

In anticipation of experimental results of the ionic strength dependence of $L_{el}$, we now describe numerical calculations of the relative electrostatic energy associated with the bent and rod configurations of a linear array of charges. The rodlike polyion is assumed to have a continuous bend along its contour length $L$. Relative to the rod configuration, the angle $\phi$ is defined by connecting bead 1 and bead $N + 1$. The distance between the 1st and $(N + 1)$th bead is the chord for an arc angle of $\theta = 2\phi$ associated with a circle of radius $R = Nb/\theta$. Using the center of the circle as the reference point, the spatial distance $b_{ij}$ between the $i$th and $j$th charged group is simply the chord length for an angle $|i - j|\phi/N$,

$$b_{ij} = b \sin(|i - j|\phi/N)/(\phi/N) \quad (39)$$

These relationships are illustrated in Figure 5. The screened Coulomb potential at site $i$ for a bend of angle $\phi$ is of the form

$$\langle V_{el}\rangle_i = (q_{net}e/\epsilon)(\phi/N)\sum_{j=1}^{N+1}{}' \exp[-b/\lambda_{DH} \times \sin(|i - j|\phi/N)]/[b \sin(|i - j|\phi/N)] \quad (40)$$

where the $'$ indicates that the term for $j = i$ is omitted in the sum. The total electrostatic interaction energy for the linear polyion bent through an angle $\theta$ is therefore

$$E_\theta = (q_{net}e/2)\sum\langle V_{el}\rangle_i \quad (41)$$

where the factor of 2 corrects for the overcounting between the pairs of sites.

The ionic strength dependence of the persistence length can be estimated from the relationship $L = L_p$ when $\theta = 68.4°$. From the results for a flexible coil one can write,

$$\ln(L_{el}) = \ln[(E_{68.4} - E_0)/kT] \quad (42)$$

A plot of $-\ln(L_{el})$ versus $-\ln(C_s)$ for the various models is given in Figure 6 along with the experimental results of the upper bound value of $L_{el}$ for the PAA-K system. For the purpose of comparison with the SF/O theories, the infinite chain length limit was approximated in our numerical calculations using the value $N + 1 = 4000$. In all of the models the power dependence $x$ of $L_{el}$ on the salt concentration, i.e., $C_s^x$, appears to approach the value $x = -1$ in the asymptotic limit to zero salt concentration. The Le Bret calculations for the conducting surface indicate that $x$ only slightly deviates from the value $-1$ over the entire salt concentration range examined. The power law is $x \sim -1/2$ in the higher salt regimes for polyions with nonconducting surfaces. The Fixman calculations follow the trend of the nonconducting surface results of Le Bret. Our calculations for the (approximate) infinite chain closely resemble the SF/O values, thus lending credibility to the current computational methods of eq 39–42.

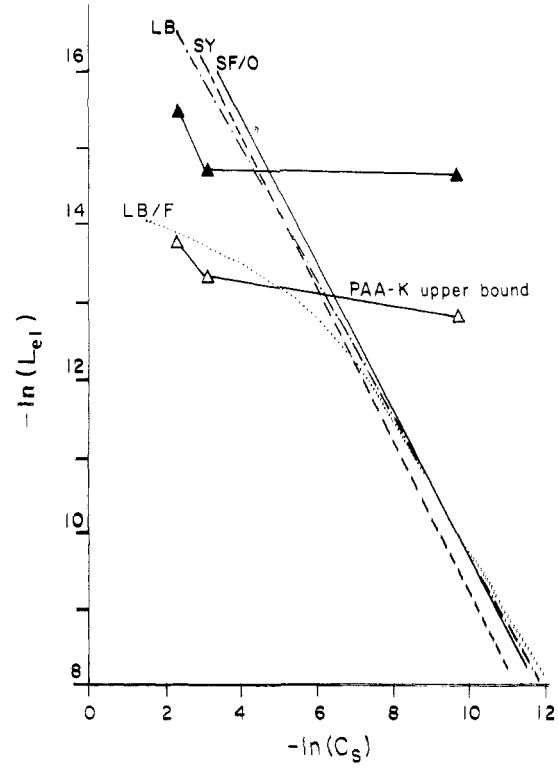


**Figure 6.** Comparison of theoretical and experimental values for the electrostatic component of the persistence length as a function of added salt: (—) (SF/O) Skolnick-Fixman[7]/Odijk[8] results with Manning condensation (eq 11); (- - -) (LB) Le Bret[15] calculations for a cylinder of radius 10 Å and a conducting surface; (···) (LB/F) Le Bret[15] and Fixman[16] calculations for a cylinder of radius 10 Å and a nonconducting surface; (- - -) (SY) calculations using eq 39–42 with $N + 1 = 4000$ and Manning condensation and $\ln(L_{el}) = \ln[(E_{68.4} - E_0)/kT]$ at 25 °C; (△) upper bound experimental values for PAA-K computed from eq 7 and 37; (▲) experimental values for PAA-K using $\nu$ computed from viscosity data in ref 28 and eq 30 and 34.

In contrast to all of the theoretical results, the experimental values of $L_{el}$ for PAA-K clearly indicate a "plateau" value for $L_{el}$ as the ionic strength is lowered. The numerical values are compared with the experimental values in Table IV. We propose that this plateau value is a direct result of the intrinsic flexible nature of the PAA and is therefore outside the range of the assumptions employed in the calculations of Le Bret and Fixman and the analytical solution for $L_{el}$ of the SF/O approach. That is, the theoretical explorations have been limited to small deviations from rodlike behavior, primarily for mathematical simplicity in the evaluation of the electrostatic interactions. The SF/O expressions therefore represent a first approximation for the flexible coil polyelectrolyte. Furthermore, it is our opinion that the elastic constant associated with bending, $\gamma_{el}$, cannot be treated on equal footing with the intrinsic elastic constant of bending, $\gamma_0$, as inferred from eq 6 and 7. This is because the interactions which are manifested in the parameter $\gamma_0$ act along the contour length of the polymer, whereas the Coulombic interactions are not transmitted along the contour length but rather directly through space.

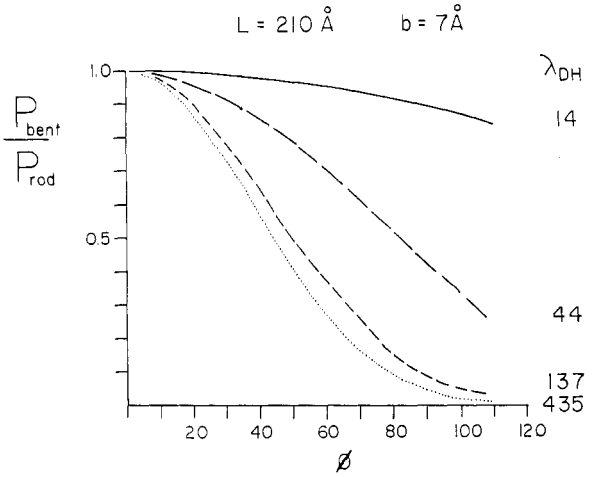


**Figure 7.** Relative probability of bent/rod configurations. The relative probability of a molecule having a smooth bend through the angle $\phi = \theta/2$ to it having the rodlike configuration is assumed to be given by $P_{bent}/P_{rod} = \exp[-(E_\theta - E_0)/kT]$, where $E_\theta$ is given by eq 41.

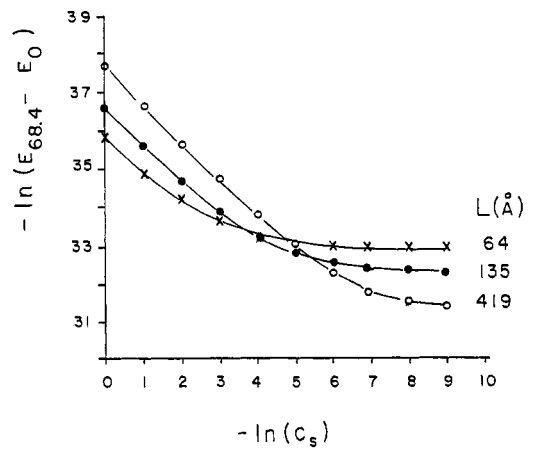


**Figure 8.** Ionic strength dependence of the electrostatic component to the persistence length for the exact pairwise screened Coulombic potential. It is assumed that the ionic strength dependence of the energy associated with an end-to-end bend through an angle of $\theta = 68.4°$ is associated with the ionic strength dependence of the persistence length. The corresponding values of the persistence lengths are given above, where $L_{el} = L$.

In the case of a flexible polyion, the intrinsic bending energy is assumed to be very small, such that $L_p \sim L_{el}$ under all ionic strength conditions. This approximation is assumed to be reasonable for the PAA-K system since $L_0 \sim 10$ Å and the experimental value of $L_{el}$ is greater than 90 Å (cf. Table IV). The relative probability for the bent to rod configurations ($b_{ij} = |i - j|b$) is given by $P(\text{bent})/P(\text{rod}) = \exp[-(E_\theta - E_0)/kT]$, and the results of these calculations incorporating Manning condensation, viz., $b = 7.1$ Å, are illustrated in Figure 7 as a function of the bending angle $\phi = \theta/2$. It is clear from these calculations that polyelectrolytes remain relatively flexible even in very low ionic solvents if the charged groups interact through space by a screened Coulomb potential. We can assess the limitations of the above approximations by comparison of the $C_s$ dependence of $L_{el}$ with the "exact" calculations of the ionic strength dependence of $L_{el}$. A plot of $-\ln[(E_{68.4} - E_0)/kT]$ versus $-\ln(C_s)$ for various lengths $L = L_{el}$ is shown in Figure 8. These curves indicate that $L_{el} \propto 1/C_s$ in accordance with the SF/O model as long as $\lambda_{DH} < L = L_{el}$ and that the curve "flattens" in a manner similar to that for the PAA-K system when $\lambda_{DH} > L = L_{el}$. It is concluded that the appropriate criterion for the validity of the SF/O expressions is that $\lambda_{DH} < L_{el}$. It is further emphasized that in setting $L_{el} = L$ in these calculations, the intrinsic part of the persistence length can be of arbitrary value. Since the inclusion of a nonzero value of $L_0$ would only act to "stiffen" the chain, our criterion for which $L_p$ is a linear function of $1/C_s$, viz., $\lambda_{DH} < L_{el}$, is more general than the SF/O models which are restricted to cases in which $L_{el} < L_0$.[10] Physically, this means that the proper "probe length" is $\lambda_{DH}$ and that the coillike polyion must be *reasonably stiff* over the distance $\lambda_{DH}$.

**Table V**
**Comparison of the Upper Bound Values for the Excluded-Volume Parameter with Viscosity Values**

| | $[KCl]_{added}$ | | |
|---|---|---|---|
| | 0.00 | 0.05 | 0.10 |
| $R_H/(R_H)_0$[a] | 5.12 | 4.19 | 3.33 |
| $\nu$[b] | 0.642 | 0.619 | 0.593 |
| $\nu$[c] | 0.610[d] | 0.590 | 0.585 |

[a] $R_H$ is the effective hydrodynamic radius calculated from the fast decay mode of the overlay histograms, and $(R_H)_0 = 609$ Å. [b] Calculated from eq 38. [c] Calculated from the intrinsic viscosity expression $[\eta] = K_p M_p^a$, where $a = 3\nu - 1$, and the values of $a$ where obtained from ref 28 for the 15 °C data. [d] Actual salt concentration was [NaBr] = 0.005 M.

Odijk[11] proposed that under certain ionic strength conditions a highly extended flexible polyelectrolyte can undergo a "collapse" to a more compact structure. The comparisons of the experimental values of $D_{app}$ for the slow and the fast decay modes indicate the possibility of a "two-phase" system for a polydisperse preparation with the unusual situation in which the *fast mode* is actually the *higher molecular weight* fraction while the *slow mode* is the *lower molecular weight* fraction. This situation obtains if the distribution in molecular weight may exhibit a range that straddles the Odijk concentration $C^*_p$ as defined by eq 13. According to Odijk,[11] the polyion may be in a highly extended form if $L < L_{el}$ and in a "collapsed" form if $L > L_{el}$. In the sample with no added salt ($C_s \sim 7 \times 10^{-5}$ M), one has according to eq 11 the value $L_{el} = 9635$ Å. If $L_{el}$ is now associated with the "critical length", then the Odijk concentration computed from eq 13 is $C^*_p = 8 \times 10^{-11}$ M. Given the mass/length ratio of 40 g/Å,[17] the molecular weight of this transition sized particle is $9635 \times 40 = 3.85 \times 10^5$ daltons, hence a concentration of $(8 \times 10^{-11}) \times (3.85 \times 10^5) = 3.12 \times 10^{-5}$ g/L. Since this concentration is less than that used for these studies (0.02 g/L), it would appear theoretically feasible in accordance with the Odijk model for rodlike and coillike conformations to coexist *under the conditions of no added salt*. This interpretation is not, however, consistent with the observations in regard to the addition of salt, where the Odijk model would predict that all of the polyions should be in the coillike configuration.

**Upper Bound to the Excluded-Volume Parameter.** It is noted that Weill and des Cloizeaux[29] suggested that, in general, the scaling exponent $\nu$ for the static property $R_G$ differs from that for the dynamic property $R_H$. These scaling exponents are equivalent in the asymptotic limit of very large polymers. This raises the question of the validity of the application of eq 30 in this exercise. It may be expected, however, that the asymptotic limit is approached, if not in fact attained, for the present PAA-K system since the smallest value of $L/L_p$ is $2.5 \times 10^5/260 \sim 962$. Assuming that this is the case for the present system, an estimate of the *upper bound* to the excluded-volume parameter was calculated from eq 38 and summarized in Table V. As these calculations indicate, the ionic strength behavior of $R_H$ can be solely interpreted in

Table VI
Ionic Strength Dependence of $L_{el}$ for PAA at 25 °C

| $[KCl]_{added}$ | $\langle R_G^2\rangle^{1/2}$ [a] | $\nu$ [b] | $L_{el}$ [c] | $L_{el}$ [d] |
|---|---|---|---|---|
| 0.00 | 4680 | 0.610 | 47.8 | |
| 0.05 | 3825 | 0.590 | 39.5 | 42 |
| 0.10 | 3045 | 0.585 | 21.1 | 30 |

[a] $\langle R_G^2\rangle^{1/2} = 1.5R_H$. [b] Calculated from $a = 3\nu - 1$, where $a$ was the reported 15 °C values in ref 28. [c] $L_{el} = L_p - L_0$, where $L_0 = 10$ Å.[17] [d] From Figure 10 of ref 17 for the completely neutralized samples of PAA, based on intrinsic viscosity data.

terms of a *slight increase* in the excluded-volume parameter.

**Estimate of the Actual Values of $L_{el}$ and $\nu$.** It is clear from the above calculations that the ionic strength dependence of $R_H$ can be interpreted solely as an increase in the persistence length or the excluded-volume parameter. In order to provide some insight as to the actual changes in these parameters, it is necessary to perform the studies as a function of molecular weight at fixed ionic strength, where $\nu$ is determined from the ratios $[\langle R_G^2(M_1)\rangle/\langle R_G^2(M_2)\rangle]^{1/2}$ and $L_p$ from the specific values of $\langle R_G^2(M_2)\rangle^{1/2}$ (cf. eq 34). It is also possible to estimate $\nu$ from viscosity measurements where, in the asymptotic chain length limit, the following relationship between the radius of gyration and the intrinsic viscosity ($[\eta]$) holds:[29]

$$[\eta] = (K'/M_p)\langle R_G^2\rangle^{3/2} = K_p M_p^{\,a} = K_p M_p^{(3\nu-1)} \quad (43)$$

where $M_p$ is the molecular weight, $K'$ is a constant, and $K_p$ is a proportionality "constant" that, in general, depends upon both $\nu$ and $L_{el}$. The persistence length can now be calculated from $R_H$ by using eq 30 and 34 where the value of $\nu$ is obtained from intrinsic viscosity data, which in this exercise comes from the 15 °C data given in the *Polymer Handbook*.[28] It is assumed that the parameter a does not significantly change between 15 and 25 °C in this analysis. The results are summarized in Table VI. These values of the persistence length are in good agreement with those reported by Kitano et al.[17] on the basis of intrinsic viscosity data on their copmpletely neutralized PAA sample, which are also summarized in Table VI.

**The Slow Mode.** As indicated in the above analysis, the slow mode cannot be interpreted in terms of the current models for polyion conformations. The presence of a slow mode in polyion solutions that cannot be interpreted in terms of the molecular dimensions has been reported for short fragments of DNA,[30-32] poly(lysine),[33,34] and poly(styrene sulfonate).[35,36] For example, in their study of sonicated mouse liver DNA in 0.001 M NaCl, Chen and Chu[30] reported that the correlation functions were characterized by two relaxation processes with decay rates that correspond to apparent diffusion coefficients of $D_{fast} \sim 6 \times 10^{-8}$ cm$^2$/s and $D_{slow} \sim 1.8 \times 10^{-8}$ cm$^2$/s. An estimate of the minimum contour length $L$ necessary to yield this value of $D_{slow}$ is obtained for a rodlike structure. Using a diameter $d = 27$ Å[37] and eq 26 yields a value of $L \sim 1.5 \times 10^4$ Å for the *sonicated DNA*, which is considerably larger than reported by Record et al.[38] in their sonication studies, viz., 153 Å $< L <$ 1545 Å. We compare the results of Chen and Chu with those of Fulmer et al.[31] for mononucleosomal DNA ($L \sim 510$ Å), in which data were collected at delay intervals of 1–2 μs (fast regime) and 10–20 μs (slow regime). These authors reported that $D_{fast} \sim D_{slow} \sim 3.0 \times 10^{-7}$ cm$^2$/s for ionic strengths above 0.05 M, whereas these relaxation times "split" for ionic strengths below 0.05 M. For mononucleosomal DNA in 0.005 M NaCl Fulmer et al.[31] reported that $D_{slow} \sim 2 \times 10^{-8}$ cm$^2$/s, which is comparable to the value of $D_{slow}$ reported by Chen and Chu.[30] The location and breadth of the "splitting" phenomenon for DNA appear to be dependent upon the length of the DNA, as inferred by the comparison of the dinucleosomal DNA results[32] with the mononucleosomal study.[31] This type of behavior may reflect congested solution conditions where particles are "trapped" within a cage composed of surrounding neighbors. In contrast, the splitting phenomenon reported for poly(lysine)[33,34] and poly(styrene sulfonate)[35,36] appears to be a function of the *monomer* concentration ($C_m$), the ionic strength ($I$), and the small ion charge ($Z_s$) in accordance with the empirical expression of Drifford and Dalbiez,[35,36]

$$C_m b/2I\lambda_B = |Z_s| \quad (44)$$

There is at present no theoretical explanation for this unusual dependence of the transition on the added salt ($Z_sI$), but it has been suggested that the Drifford–Dalbiez ratio reflects the onset of overlap of volumes for the monomer and the ion cloud.[39] The slow mode for the PAA-K system may well reflect these overlap conditions. Given the molecular weight of $10^7$ and the concentration 0.02 g/L, the average distance between cubic cells is ~10 000 Å, which compares to the hydrodynamic diameter $2R_H \sim 6200$ Å, or $2\langle R_G^2\rangle^{1/2} = 9300$ Å, under zero added salt conditions. Since $\gamma_{slow}/K^2$ (cf. Table II) and $\Delta/K^2$ (cf. Table III) are independent of $K$, the slow relaxation process is to be associated with translational diffusion. We suggest, therefore, that $D_{slow}$ observed for the present system is due to the hindered diffusion of PAA-K molecules through cages composed of neighboring PAA-K molecules. These two regimes are schematically represented in Figure 9.

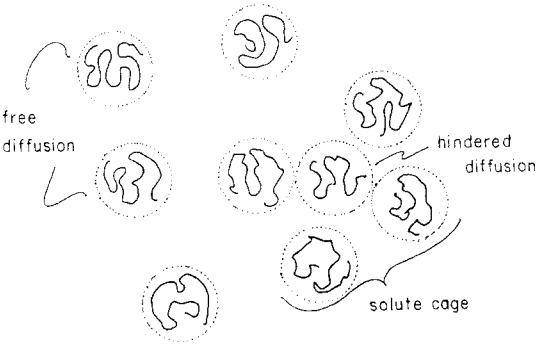


**Figure 9.** Schematic representation of the two diffusion regimes. The decay rates for the two modes are proportional to $K^2$, as expected for translational diffusion. The bimodal distribution is interpreted in terms of free and hindered diffusion regimes. Although the figure depicts these two regimes as spatially distinct regions, it is emphasized that the solute cages are continually being formed and disrupted. Hence, the two relaxation modes may actually reflect the time evolution of the diffusion process for the probe particle. That is, the early part of the relaxation curve takes place on a time scale in which the solute particle has not traveled far from its initial position whereas the latter part of the decay curve reflects larger diffusion distances in which the probe particle has now encountered several other solute particles that hinder the movement of the probe particle.

**QELS versus $I_{tils}$ Determination of $\langle R_G^2\rangle^{1/2}$.** Since our estimates of the persistence length and the excluded-volume parameters are based on the calculated values of the radius of gyration through eq 30, the question arises as to why $\langle R_G^2\rangle^{1/2}$ is not obtained directly from total intensity light scattering ($I_{tils}$) measurements by making Zimm plots. In this procedure $I_{tils}$ is measured as a function of polyion concentration ($C_p$) and scattering vector, where $\langle R_G^2\rangle$ is obtained directly from the initial slope of $1/I_{tils}$ ($C_p = 0$) versus $K^2$. While this procedure is preferred in theory, it may not be possible to achieve in practice due to the uncertainties in the extrapolated

values to zero concentration. This is due to the low intensity of scattered light and the intrinsically nonideal nature of polyelectrolyte systems. For example, Hara and Nakajima reported $I_{tils}$ studies on dilute[27] and semidilute[40] solutions of PAA of molecular weights $M_p = 1.1 \times 10^5$ and $3.9 \times 10^5$, which are considerably smaller than those used in the present study ($M_p = 1 \times 10^7$). Under all salt conditions examined, these authors reported nonzero second virial coefficients which were larger than those generally obtained for neutral polymers. More important, linear plots were obtained only under the most dilute polyion concentrations and relatively high added salt conditions ($C_s > 0.1$ M). Anomalous plots exhibiting strong curvature were obtained for lower ionic strength solvents. It is anticipated that the current system would exhibit grossly distorted Zimm plots at these added salt concentrations, even though the concentration used in the present study ($C_p \sim 0.02$ g/L) are less than those in the studies of Hara and Nakajima ($C_p > 0.2$ g/L). This is because the particle volume fraction $\phi_p$ of PAA-K in the present study is greater than that used by Hara and Nakajima, as estimated by the ratio under $\Theta$ conditions, $\phi_p \propto \langle R_G^2 \rangle^{3/2} C_p \propto M_p^{3/2} C_p$. One has for these two systems $(M_1/M_2)^{3/2}[(C_p)_1/(C_p)_2] = [(1 \times 10^7)/(1 \times 10^5)^{3/2}\ (0.02/0.2) = 100$. It is of interest to note that these authors attribute the highly anomalous behavior in the semidilute region as a manifestation of "lumps of molecules" as opposed to the formation of microgels. These "lumps of molecules" may correspond to the anomalous slow mode evident in the overlay histograms observed for the present system. If this correspondence is correct, then a distinct advantage of using QELS techniques over $I_{tils}$ methods for highly charged macroions in low ionic strength solvents is the kinetic separation of the "normal" and "abnormal" contributions to the total scattered light. It is also for this reason that the cumulant method of analysis may lead to an overestimate of the polyion hydrodynamic radius since $K_1$ measures the average of both processes.

## Conclusions

What emerges from this study and those in the literature is that PAA-K in aqueous solutions behaves like a flexible coil in a "good solvent" whose equivalent hydrodynamic dimensions increase upon lowering the ionic strength, where the expansion process is governed by a modest increase in both the excluded-volume parameter $\nu$ and in the electrostatic persistence $L_{el}$. It is further concluded from both the experimental data and numerical calculations using a screened Coulomb potential as presented in this study that there exists an *upper limit* to $L_{el}$. The presence of an upper limit to $L_{el}$ is related to the intrinsic flexibility of the linear chain and the relatively short-range nature of a screened Coulomb potential. Quantitatively, an upper limit to $L_{el}$ may be expected if the electrostatic "probe length" as approximated by the Debye–Hückle length $\lambda_{DH}$ exceeds the electrostatic component of the persistence length of the chain, viz., $\lambda_{DH}/L_{el} > 1$. Physically this means that the polyion does not appear as "rodlike" over the range of the screened Coulomb interaction and that any additional repulsive interaction energy which comes into play as the ionic strength is lowered is not of sufficient magnitude to overcome the thermal energy $kT$. These results are in very good agreement with the first-order correction models of Skolnick and Fixman[7] and of Odijk[8] and the calculations of Le Bret[15] and Fixman[16] within the constraint of *small deviations* from the rodlike structure.

**Acknowledgment.** This research was partially supported by a Weldon Springs grant from the Research Council of the University of Missouri—Kansas City. We gratefully acknowledge the comments made by the reviewers of this manuscript.

**Registry No.** PAA-K, 25608-12-2.

## References and Notes

(1) Manning, G. S. *J. Chem. Phys.* **1969**, *51*, 924.
(2) Manning, G. S. *Biopolymers* **1972**, *11*, 951.
(3) Manning, G. S. In *Polyelectrolytes*; Selegny, E., Ed.; Reidel: Dordrecht, Holland, 1974.
(4) Manning, G. S. *Biophys. Chem.* **1977**, *7*, 95.
(5) Manning, G. S. *Q. Rev. Biophys.* **1978**, *11*, 179.
(6) Russel, W. B. *J. Polym. Sci.* **1982**, *20*, 1233.
(7) Skolnick, J.; Fixman, M. *Macromolecules* **1977**, *10*, 944.
(8) Odijk, T. *J. Polym. Sci., Polym. Phys. Ed.* **1977**, *15*, 477.
(9) Yamakawa, H. In *Modern Theory of Polymer Solutions*; Harper and Row: New York, 1971; Section 9.
(10) Odijk, T.; Houwaart, A. C. *J. Polym. Sci., Polym. Phys. Ed.* **1978**, *16*, 627.
(11) Odijk, T. *Macromolecules* **1979**, *12*, 688.
(12) Zimm, B. H.; Le Bret, M. *J. Biomol. Struct. Dynam.* **1983**, *1*, 461.
(13) Le Bret, M.; Zimm, B. H., *Biopolymers* **1984**, *23*, 287.
(14) Klein, J.; Ware, B. R. *J. Chem. Phys.* **1984**, *80*, 1334.
(15) Le Bret, M. *J. Chem. Phys.* **1982**, *76*, 6243.
(16) Fixman, M. *J. Chem. Phys.* **1982**, *76*, 6346.
(17) Kitano, T.; Taguchi, A.; Noda, I.; Nagasawa, M. *Macromolecules* **1980**, *13*, 57.
(18) Kim, O.-K.; Long, T.; Brown, F. *Polym. Commun.* **1986**, *27*, 71.
(19) Koppel, D. E. *J. Chem. Phys.* **1972**, *57*, 4814.
(20) Fletcher, G. C.; Ramsay, D. J. *Opt. Acta* **1983**, *30*, 1183.
(21) Pecora, R. *J. Chem. Phys.* **1968**, *48*, 4126.
(22) Garcia de la Torre, J.; Bloomfield, V. A. *Q. Rev. Biophys.* **1981**, *14*, 81.
(23) Zimm, B. *J. Chem. Phys.* **1956**, *24*, 279.
(24) Pecora, R. *J. Chem. Phys.* **1968**, *49*, 1032.
(25) Tivant, P.; Turq, P.; Drifford, M.; Magdelenat, H.; Menez, R. *Biopolymers* **1983**, *22*, 643.
(26) Sharp, P.; Bloomfield, V. A. *Biopolymers* **1968**, *6*, 1201.
(27) Hara, M.; Nakajima, A. *Polym. J.* **1980**, *12*, 701.
(28) Brandrup, J.; Immergut, E. H., Eds. *Polymer Handbook*, 2nd ed.; Wiley-Interscience: New York, 1975; p IV-9.
(29) Weill, G.; des Cloizeaux, J. *J. Phys. (Les Ulis, Fr.)* **1979**, *40*, 99.
(30) Chen, F. C.; Chu, B., *J. Chem. Phys.* **1977**, *66*, 2235.
(31) Fulmer, A. W.; Benbasat, J. A.; Bloomfield, V. A. *Biopolymers* **1981**, *20*, 1147.
(32) Schmitz, K. S.; Lu, M. *Biopolymers* **1984**, *23*, 797.
(33) Lin, S.-C.; Lee, W. I.; Schurr, J. M. *Biopolymers* **1978**, *17*, 1041.
(34) Zero, K.; Ware, B. R. *J. Chem. Phys.* **1983**, *80*, 1610.
(35) Drifford, M.; Dalbiez, J.-P. *J. Chem. Phys.* **1984**, *88*, 5368.
(36) Drifford, M.; Dalbiez, J.-P. *J. Phys. Lett.* **1985**, *46*, L311.
(37) Elias, J. G.; Eden, D. *Biopolymers* **1981**, *20*, 2369.
(38) Record, M. T., Jr.; Woodbury, C. P.; Inman, R. B. *Biopolymers* **1975**, *14*, 393.
(39) Schmitz, K. S.; Ramsay, D. J. *J. Colloid Interface Sci.* **1985**, *105*, 388.
(40) Hara, M.; Nakajima, A. *Polym. J.* **1980**, *12*, 711.